# Cluster-Based Solidification and Growth Algorithm for Decagonal Quasicrystals

P. Kuczera and W. Steurer
*Laboratory of Crystallography, ETH Zurich, CH-8093 Zurich, Switzerland*
(Received 7 January 2015; revised manuscript received 13 May 2015; published 21 August 2015)

A novel approach is used for the simulation of decagonal quasicrystal (DQC) solidification and growth. It is based on the observation that in well-ordered DQCs the atoms are largely arranged along quasiperiodically spaced planes parallel to the tenfold axis, running throughout the whole structure in five different directions. The structures themselves can be described as quasiperiodic arrangements of decagonal columnar clusters (cluster covering) that partially overlap in a systematic way. Based on these findings, we define a cluster interaction model within the mean field approximation, with effectively asymmetric interactions ranging beyond the nearest neighbors. In our Monte Carlo simulations, this leads to a long-range ordered quasiperiodic ground state. Indications of two finite-temperature unlocking phase transitions are observed, and are related to the two fundamental length scales that are characteristic for the system.

DOI: 10.1103/PhysRevLett.115.085502 PACS numbers: 61.44.Br, 61.43.Bn, 61.50.Ks

Two fundamental questions remain open in our understanding of quasicrystals (QCs). One question regards how QCs grow, and the other refers to their main stabilization mechanism. The discussion about energy versus entropy stabilization has been ongoing ever since the discovery of QCs [1]. "Energy-stabilized" QCs would have a quasiperiodic ground state, while "entropy-stabilized" QCs would be quasiperiodic on average only at sufficiently high temperatures ($T$), and would transform into periodic approximant structures at low $T$. If a tiling or covering of a QC obeys matching or overlap rules, respectively, it is a proof that it is strictly quasiperiodic. This does not work the other way around; neither matching rules for tiles nor overlap rules for clusters are growth rules. There were some attempts, however, to circumvent this problem. For example, one model [2] allows us to grow a 2D Penrose tiling from a single "decapod defect." This idea has also been extended to a 3D layer model [3]. Classical matching rules can also be replaced by the requirement of maximizing the density of specific tile clusters [4]. For dynamic models, it has been demonstrated both theoretically [5] and by Monte Carlo (MC) simulations [6,7] that finite-$T$ quasiperiodic long-range order (LRO) cannot be achieved in 2D systems with local interactions only (matching or overlap rules). The 2D local-interactions-based systems are, therefore, in a so-called *unlocked* state at any finite $T$. The structure of such unlocked phases can be described by random tiling models [8–10], with only on-average quasiperiodic order. For 3D layer models of decagonal quasicrystals (DQCs) based on local interactions, an unlocking phase transition is observed at finite $T$ [11,12]. The locked phase exhibits true quasiperiodic LRO. An interesting result for 2D systems was recently obtained by molecular dynamics (MD) simulations with a two-minima radially symmetric Lenard-Jones-Gauss potential [13], which resulted in an entropy-stabilized DQC transforming into an approximant at low $T$.

We use a completely different approach, which is based on some fundamental experimental observations: (i) DQCs show distinct cluster structures, with the atomic decoration of these clusters breaking the tenfold symmetry [14–18]. (ii) Even rapidly solidified quasicrystals exhibit a good LRO; therefore, it is reasonable to assume that clusterlike arrangements of atoms exist already in the melt close to the solidification temperature (see, e.g., [19]). (iii) The atoms in DQCs are arranged on quasperiodically spaced flat atomic layers parallel to the tenfold axis [20]. (iv) DQCs are not layer structures in the crystal-chemical meaning, because the chemical bonding within the quasiperiodic layers does not differ from the chemical bonding between them. Therefore, as also indicated by their growth morphology, the structures of DQCs should be described in terms of systematically partially overlapping 3D columnar clusters instead of a stacking of quasiperiodic layers [20,21].

Most experimentally derived DQC structure models published so far have essentially the same building principles: Decagonally shaped columnar clusters (of diameter $\approx$20 Å or $\tau$ inflated with $\tau \approx 1.618$, the golden mean) decorate the vertices of a decagonal ($d$) tiling [in most cases a pentagonal Penrose tiling (PPT)], thereby forming a covering. Figure 1(a) shows an example of such overlapping decagonal clusters overlaying an electron density map of $d$-Al-Cu-Rh [18] projected along the tenfold axis. For a closer look, let us focus on one cluster, for instance, the red one. The thin lines mark the traces of the quasilattice planes (QLPs), which intersect the rhomb Penrose tiling (RPT), outlined by thick black lines, in a specific way. The properties of these particular sets of lines in the RPT, which are not equivalent to the Ammann or de Bruijn lines, were

 

previously demonstrated by Hoffman and Trebin [22]. The RPT, with an edge length of $a \approx 4$ Å, nicely matches the strong electron density maxima. Each electron density maximum is intersected by at least two QLPs; most heavy atom maxima are crossed by five QLPs. There are three typical interplanar distances between the QLPs: $d_1$, $d_2$, and $d_3$ [$d_1 = 0.5a(3-\tau)^{0.5}$, $d_2 = d_1/\tau$, and $d_3 = d_2/\tau$]. Every second distance is $d_2$; distances $d_1$ and $d_3$ occur according to the Fibonacci sequence. The RPT outlined in black, and thus the sets of QLPs outlined by thin red lines, originate at the point indicated by the red filled circle on the cluster boundary. In total there are 99 QLPs decorating each cluster. The arrangement of QLPs within a cluster, like the atomic decoration, exhibits only mirror symmetry. The thin black lines in Fig. 1(a) illustrate how the QLPs run from cluster to cluster throughout the structure. It is, therefore, obvious that in the growth process of a DQC the atoms arrange themselves along the QLPs, which is exactly what can be observed experimentally in grown DQCs. New clusters added to the structure continuously extend the existing QLPs and are the origin of the new QLPs as well. The growth morphology of DQCs is also determined by the QLPs.

Now let us focus on the coarse-grained cluster model, which consists of regular decagons decorated with five sets of QLPs as illustrated in Fig. 1(a). Because the cluster decoration reduces the tenfold symmetry to just mirror symmetry, ten possible orientations of each cluster result. Our basic assumption underlying the simulations is that it is energetically most favorable for the clusters to arrange themselves in a way that the maximum number of QLPs is continued from cluster to cluster (the "QLP continuation rule"). Discontinuations of QLPs increase the system energy. This approach differs significantly from the matching-rule approach, because a QLP originating from a given cluster extends beyond the cluster up to a certain (adjustable) range. Therefore, it can influence more than just the nearest-neighbor clusters. In our model, the clusters interact through a QLP field, which is constructed within the mean field approximation (MFA). The QLPs defined for a single cluster extend beyond the cluster; thus, it can be said that each cluster is a source of a QLP field. In turn, every cluster interacts with the average QLP field produced by other clusters, whose QLPs extend to its position. The energy of each cluster is defined as the number of mismatches between the QLPs in the given cluster and the QLP field. Note that the QLP field produced by a cluster is strongly dependent on the cluster orientation; this is fundamentally different from the approach in Ref. [13], where the interaction potential is radially symmetric.

Assuming that in the fully ordered DQC the clusters are centered at the vertices of a perfect PPT, there are two typical intercluster distances whose ratio is equal to $\tau$. To define the length scale of our model, we fix those distances to be 1 and $\tau^{-1}$. In such a case, the edge length of the PPT is fixed to 1, and the radius of the cluster (the center-to-vertex distance), as well as the edge length of the underlying RPT, is fixed to $a = (3-\tau)^{-0.5} \approx 0.851$ [Fig. 1(b)]. For the indexing of the cluster vertices, we use the 5D hypercubic basis of the 2D PPT. The basis vectors form a pentagonal star, $\mathbf{a}_i = a(\cos(i2\pi/5), \sin(i2\pi/5)), i = 1,2,\ldots,5$. Using this basis, any vertex of the PPT can be indexed with a

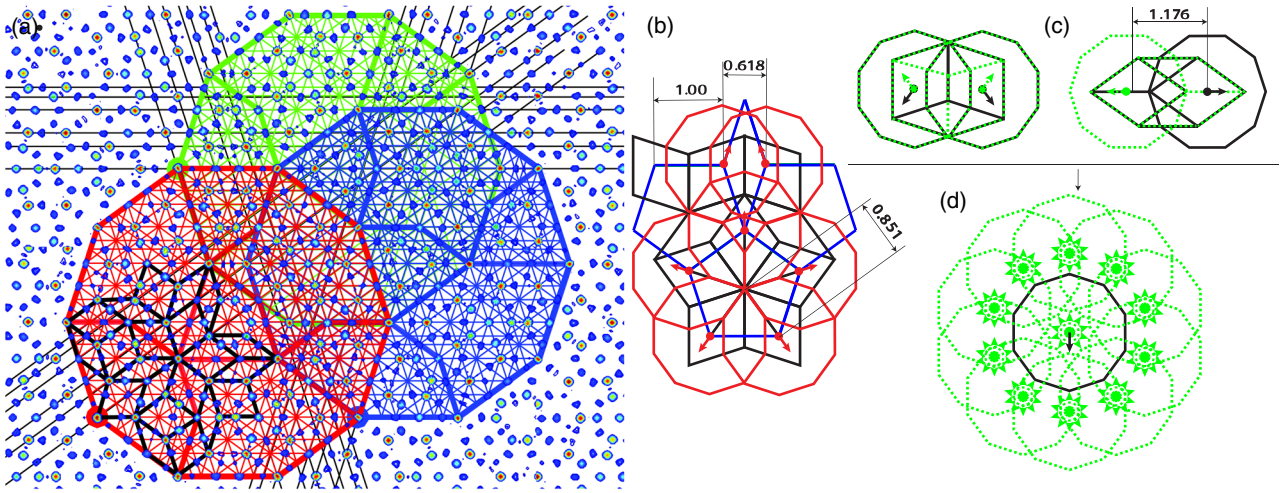


FIG. 1 (color online). (a) Clusters of size 32 Å overlaying a part of the electron density of *d*-Al-Cu-Rh [18]. The thin lines, marked in the respective colors, indicate the QLPs in the clusters. *For example,* in the red cluster, the red filled circle indicates the origin point of RPT outlined in black and the QLPs. The thick lines inside each cluster correspond to the Gummelt overlap rules [23]. The thin black lines illustrate how the QLPs are continued from cluster to cluster throughout the structure. (b) The ideal PPT is outlined in blue, the ideal underlying RPT in black, and the decagonal clusters in red (arrows indicate cluster orientations). (c) Two possible hexagonal RPT flip arrangements. The black contours indicate the original arrangements, the broken green lines the flipped ones. (d) A generalized cluster flip as used in this Letter.

quintuplet of integer indices, $h_i$, which corresponds to a subset of a $\mathbb{Z}$-module of rank 5. For any vertex, $(\sum_{i=1}^{5} h_i)\mathrm{mod}5 = 1$. A quasiperiodic structure can be rearranged by cluster flips. There are two typical hexagonal "flip arrangements" in RPT, shown in Fig. 1(c). In the case of the skinny hexagon arrangement (two thin rhombs and one thick rhomb), the tile flip corresponds to a cluster jump and reorientation. In the case of fat hexagon arrangement (two thick rhombs and one thin rhomb), the flip corresponds only to a reorientation of the clusters. The length of the cluster jump is equal to $a^{-1} = (3-\tau)^{0.5} \approx 1.176$. In our model we use a somewhat generalized notion of cluster flip, illustrated in Fig. 1(d). In a single update step, a cluster can either be reoriented at its original position or be flipped to one of ten surrounding positions, each having ten possible orientations. Such generalized cluster flips ensure that our model is, in principle, not equivalent to a tiling model. The flips are not restricted to specific tile arrangements underlying the cluster structure. The indices of a vector describing a cluster flip fulfill the following equation: $(\sum_{i=1}^{5} h_i)\mathrm{mod}5 = 0$. Flips can create intercluster distances, which are not found in a fully ordered structure. We limited the shortest possible distance in the simulations to $\tau^{-1}$.

For our MC simulations, we used a circular simulation box with free boundary conditions. In the first approach, called model 1, we studied two different system sizes with radii of 12 and 22 [in the defined length scale, see Fig. 1(b)] and assumed that the QLPs originating in any cluster run through the whole simulation box–infinite interaction range limit. The amount of clusters was fixed to the number of vertices of a perfect PPT for a given system size. In our case, there were 465 and 1585 clusters for the two studied system sizes, respectively. In the second approach, called model 2, we limited the range or QLPs originating in a given cluster to the distance of 3, counting from cluster's origin (in the defined length scale). In this case the interactions are not infinite range, but reach beyond the nearest neighbors. We studied only the smaller system size, i.e., with a radius of 12 and 465 clusters, since the calculations are much more time consuming (the set of clusters contributing to mean field changes for every potential new cluster position and, thus, the mean field has to be calculated from scratch). For model 2 another assumption has to be made as well. In high $T$ the cluster orientations might not yet be definite due to high atom mobility. To simulate this, we let a cluster in each position have two orientations (they can be the same but this is not required). The QLP field produced by a cluster is, then, an average of the fields produced by the given cluster in the two orientations. In low $T$ the two orientations will coincide. Under such assumptions, model 2 leads to essentially the same results as model 1.

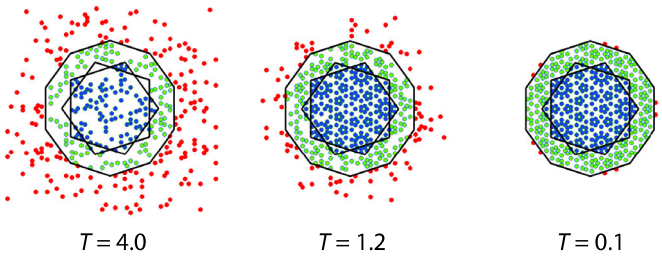


FIG. 2 (color online). Snapshots of the simulated structure for model 1 in perpendicular space at different temperatures. The disordered clusters are marked in red. Properly ordered $L$-sublattice clusters occupy a double-pentagonal region inside the decagonal AS, and are marked in blue. Properly ordered $S$-sublattice clusters are occupying the region inside the decagon but outside the pentagon, and are marked in green.

The simulation started with a structure randomization at high temperature, allowing the formation of gaps between clusters. Then, the system behavior was studied upon systematic cooling. After initial equilibration at every temperature step, in each MC sweep, we first determine the QLP mean field from the current cluster arrangement. For each cluster, in random order, we calculate its energy ($E_i$) in all states that are geometrically available within the generalized flip (a potential new position cannot be occupied, and also no position within a radius of $\tau^{-1}$ from it can be occupied). The probability of cluster's transition to the $i$th accessible state can be written as $P_i \propto \exp(-E_i/kT)$; this is the heat-bath algorithm.

An ideal PPT can be obtained by the projection of a subset of the vertices of a properly oriented 5D hypercubic lattice onto parallel space selected by a decagonal window (the so-called atomic surface, AS) in perpendicular space. In other words, all the vertices of a PPT in parallel space correspond to points located in a decagon in perpendicular space. Therefore, if a cluster flips to a position that does not belong to the perfect PPT, its corresponding point in perpendicular space jumps out of the AS. A possible order parameter (OP) can be defined as a fraction of all the cluster centers whose positions in perpendicular space lie within the AS. For a completely ordered system OP $= 1$, and for completely disordered system at infinite $T$ and infinite system size OP $\to 0$. An ideal PPT can be subdivided into two interpenetrating sub(quasi)lattices, the first with the shortest intercluster distance equal to 1, hereafter called $L$-sublattice, and the second with the shortest intercluster distance equal to $\tau^{-1}$, hereafter called $S$-sublattice. In Fig. 2, snapshots of the simulated structures for model 1 at different temperatures are shown in perpendicular space. The decagonal AS is outlined in black, and disordered clusters are marked in red. Properly ordered $L$-sublattice clusters occupy a double-pentagonal region inside the decagonal AS, and are marked in blue. Properly ordered $S$-sublattice clusters are occupying the region inside the decagon but outside the double pentagon, and are marked in green. It is clear that the two sublattices order separately. At $T = 4$ the structure is

disordered. However, at $T = 1.2$ the $L$-sublattice is already fully ordered, whereas the $S$-sublattice is still disordered. At $T = 0.1$ both sublattices are fully ordered. Four videos, showing the ordering of the simulated structures at different temperatures, are available as Supplemental Material [24] (Videos 1–3 show model 1, Video 4 shows model 2). The color code in Videos 1 and 2 is the same as in Fig. 2; the videos show simulations for the two different system sizes, respectively. In these two simulations, the nucleus is formed by 20 clusters at the origin of the simulation box with fixed positions and orientations. This is not a requirement of the simulations, but it fixes the origin of the simulation box, which is necessary for following the order parameter throughout the simulation. Video 3 shows a simulation without such a seed. In this case, the origin of the grown structure in perpendicular space, and therefore the location of the AS, is not known *a priori*, and varies for every run of the simulation (it is only fixed below the phase transition point for a given sublattice). In Video 3, the color code from Video 1 is only applied at $T$s below the suspected unlocking phase transitions. The final result is the same: the structure is fully ordered and its image in perpendicular space is nicely decagonal. Video 4 shows the ordering phenomenon for model 2. In high $T$ the allowed two cluster orientations mostly do not coincide. However, as the $T$ decreases, both allowed cluster orientations tend to be the same. It is also clear that the $L$-sublattice orders at higher $T$ compared to model 1. In all the videos it is apparent that, as mentioned before, the randomized high-$T$ structure has voids; this is because the model is not equivalent to tiling models due to the generalized flip.

In Fig. 3, the OP and its susceptibility curves $[\chi = N(1/T)(\langle \mathrm{OP}^2 \rangle - \langle \mathrm{OP} \rangle^2)]$ versus $T$ are shown for the two sublattices separately for model 1 (left) and model 2 (right). Naturally, the OP for the two sublattices is defined as a fraction of cluster centers, whose perpendicular space coordinates lie within the appropriate subregion of the AS. The symbol $N$ in the definition of susceptibility refers to the number of clusters belonging to a given sublattice in the fully ordered case. The color code is the same as in Fig. 3; i.e., the curves related to the $L$-sublattice are marked in blue and those related to $S$-sublattice are in green. Based on the susceptibility maxima, indications of two phase transitions are visible. The structure has three distinct ordering regimes. In high $T$ both sublattices are disordered. Then, as the temperature goes down, the $L$-sublattice orders at $T \approx 2.1$ for model 1 and at $T \approx 3$ for model 2. At sufficiently low (but finite) $T$, the $S$-sublattice orders (around $T \approx 0.9$ for both models). The energy versus $T$ curves are smooth for both models, which suggests that the possible phase transitions would have a continuous character.

Based on the concept of QLPs, we have built a cluster interaction model using the MFA. Effectively, the local information about a cluster's position and orientation is mediated by the QLPs beyond the nearest neighbors (across the whole structure in model 1 and up to $r = 3$ for model 2). The interactions for both models strongly depend on the cluster orientations. These two facts significantly distinguish our approach both from MD studies with radially symmetric double-well potentials and from MC studies based on matching (overlap) rules that are local. While the MD studies lead to entropy stabilized quasiperiodic structures at high $T$ and periodic ground state, the MC studies give the LRO quasiperiodic structures only at $T = 0$ and entropy stabilized structures at any finite $T$ (in 2D). Our model leads to self-assembly of decagonal clusters into a long-range ordered quasiperiodic structure at finite $T$. Admittedly, for model 2 additional (physically feasible) assumptions are necessary to obtain self-assembly: Two possible orientations of each cluster are allowed to account for the fact that in high $T$ the cluster orientation might be not yet definite. The reason why such an assumption would cause the system to self-assemble to a LRO quasiperiodic structure in the case of finite-range interactions is unclear; however, we suspect that it has something to do with the

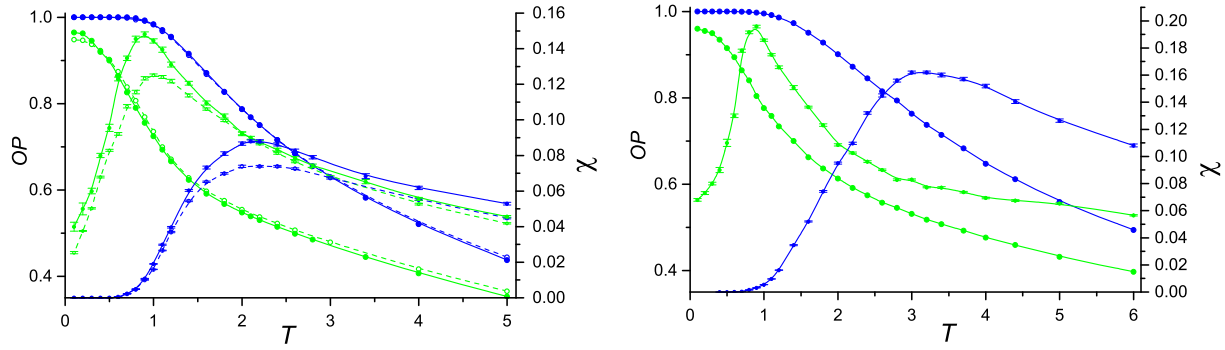


FIG. 3 (color online). (Left) Order parameters and susceptibility curves for model 1: Results for the simulation with 465 clusters are shown with dashed lines and open circles, and results for the simulation with 1585 clusters are shown with solid lines and full circles. Blue curves correspond to the $L$-sublattice (230 clusters for the smaller system and 775 for the larger system) and green curves to the $S$-sublattice (235 clusters for the smaller system and 810 for the larger system). (Right) Order parameters and susceptibility curves for model 2, in which only the smaller system size was studied.

behavior of system entropy with $T$. Note that our model is not a "templated" growth approach, because the QLP field is recalculated after each cluster flip, and that the Gummelt-like overlap rules in the ordered structure have an *emergent* character; i.e., they are a result and not a prerequisite of the model. The quasiperiodic state is here a ground state, stable down to $T = 0$. The model presented in this Letter is, of course, greatly simplified. However, we believe the formation of QLPs to be crucial during DQC growth, as it is responsible for the propagation of quasiperiodic LRO.

This project was supported by the Swiss National Science Foundation under Grant No. 200021-153559. We would like to thank Marek Mihalkovic and Marc de Boissieu for useful comments. P. K. is grateful to G. Dan Miron for fruitful discussions.

[1] D. Shechtman, I. Blech, D. Gratias, and J. W. Cahn, Phys. Rev. Lett. **53**, 1951 (1984).
[2] G. Y. Onoda, P. J. Steinhardt, D. P. DiVincenzo, and J. E. S. Socolar, Phys. Rev. Lett. **60**, 2653 (1988).
[3] H. C. Jeong, Phys. Rev. Lett. **98**, 135501 (2007).
[4] H. C. Jeong and P. J. Steinhardt, Phys. Rev. B **55**, 3520 (1997).
[5] P. A. Kalugin, Pis'ma v Zh. Eksp. Teor. Fiz. **49**, 406 (1989) [JETP Lett. **49**, 467 (1989)].
[6] L. H. Tang and M. V. Jaric, Phys. Rev. B **41**, 4524 (1990).
[7] M. Reichert and F. Gahler, Phys. Rev. B **68**, 214202 (2003).
[8] C. L. Henley, J. Phys. A **21**, 1649 (1988).
[9] M. Widom, D. P. Deng, and C. L. Henley, Phys. Rev. Lett. **63**, 310 (1989).
[10] L. J. Shaw and C. L. Henley, J. Phys. A **24**, 4129 (1991).
[11] H. C. Jeong and P. J. Steinhardt, Phys. Rev. B **48**, 9394 (1993).
[12] M. Reichert and A. Gahler, arXiv:cond-mat/0302074.
[13] A. Kiselev, M. Engel, and H. R. Trebin, Phys. Rev. Lett. **109**, 225502 (2012).
[14] P. J. Steinhardt, H. C. Jeong, K. Saitoh, M. Tanaka, E. Abe, and A. P. Tsai, Nature (London) **396**, 55 (1998).
[15] W. Steurer, Philos. Mag. **86**, 1105 (2006).
[16] W. Steurer and S. Deloudi, Structural chemistry **23**, 1115 (2012).
[17] E. Abe, Chem. Soc. Rev. **41**, 6787 (2012).
[18] P. Kuczera, J. Wolny, and W. Steurer, Acta Crystallogr. Sect. B **68**, 578 (2012).
[19] E. Abe and A. P. Tsai, J. Alloys Compd. **342**, 96 (2002).
[20] W. Steurer, Z. Anorg. Allg. Chem. **637**, 1943 (2011).
[21] W. Steurer and S. Deloudi, C.R. Phys. **15**, 40 (2014).
[22] S. Hoffmann and H. R. Trebin, Phys. Status Solidi B **174**, 309 (1992).
[23] P. Gummelt, Geometriae Dedicata **62**, 1 (1996).
[24] See Supplemental Material at http://link.aps.org/supplemental/10.1103/PhysRevLett.115.085502 for videos presenting the simulations.